Journal of
Materials Chemistry B

Materials for biology and medicine

Accepted Manuscript

This article can be cited before page numbers have been issued, to do this please use: Q. Wang, X. Zhu, Z. Wu, T. Sun, W. Huang, Z. Wang, X. Ding, J. Chen and F. Li, *J. Mater. Chem. B*, 2020, DOI: 10.1039/D0TB00017E.

ROYAL SOCIETY OF CHEMISTRY

rsc.li/materials-b

View Article Online
DOI: 10.1039/D0TB00017E

ARTICLE

Theranostic nanoparticles escorting phosphorylated gemcitabine for advanced pancreatic cancer therapy

Received 00th January 20xx,
Accepted 00th January 20xx

DOI: 10.1039/x0xx00000x

Qingbing Wang[a,b], Xingjun Zhu[b], Zhiyuan Wu[a], Tao Sun[c], Wei Huang[a], Zhongmin Wang[a], Xiaoyi Ding[a], Chen Jiang*[c] and Fuyou Li*[b]

Gemcitabine (GEM) has been the recommended first-line drug for patients with pancreatic ductal adenocarcinoma cancer (PDAC) since twenty years. However, GEM-based treatment has failed in many patients because of the drug resistance acquired in tumorigenesis and development. To override resistance to GEM in pancreatic cancer, we developed a visualisable, photothermally controlled, drug release nanosystem (VPNS). This nanosystem has $NaLuF_4$:Nd@$NaLuF_4$ nanoparticles as the luminescent core, octabutoxyphthalocyanine palladium (II) (PdPc) as the photothermal agent, and phosphorylated gemcitabine (pGEM) as the chemodrug. pGEM, one of the active forms of GEM, can circumvent the insufficient activation of GEM in cancer cell metabolism. $NaLuF_4$:Nd@$NaLuF_4$ nanoparticles were employed to visualise the tumor lesion *in vivo* by its near-infrared luminescence. The near-infrared light-triggered photothermal effect from PdPc could trigger the release of pGEM loaded in a thermally responsive ligand, and simultaneously enable photothermal cancer treatment. This work presents an effective method that suppresses the growth of tumour cells with dual-mode treatment and enables the improved treatment of orthotopic nude mice afflicted by pancreatic cancer.

1. Introduction

Pancreatic ductal adenocarcinoma (PDAC) exhibits the most dismal prognosis among all solid tumours, causing the deaths of 330,400 patients worldwide[1]. Most patients with pancreatic cancer remain asymptomatic until an advanced stage of the disease[2, 3]. The 5-year survival rate of PDAC has only increased from 3% to 7%, despite advances in molecular research, diagnostic methods, and clinical management of pancreatic cancers over the past 40 years[4]. Thus, there is significant demand for the development of novel therapeutic strategies and protocols.

Surgical resection, combined with systemic chemotherapy, offers the only hope for a cure or long-term survival for patients with pancreatic cancer[5]. However, only 10% of patients are diagnosed with PDAC that can be removed using standard resection[6]. Over the past 20 years, gemcitabine (GEM) has been the recommended as a first-line drug for patients with PDAC and is administered in conjunction with other agents, although this treatment results in only minor benefits, with an increased survival length of only 5 weeks[7-11]. Many patients suffer from GEM-based treatment failure because of drug-resistance acquired during tumorigenesis and development [12].

Several factors are related to GEM resistance for patients with pancreatic cancer. First, in terms of the parent drug, the transformation of GEM into the monophosphate form, which will be phosphorylated again to its final active metabolites, is rather limited[13]. Second, pancreatic cancer is characterized by excessive desmoplastic stroma in the tumour microenvironment, which increases solid stress inside the tumours, compresses tumour blood vessels, and limits perfusion of drugs, which increases the effective treatment concentration in cancer cells[14, 15]. Finally, cancer cell heterogeneity introduces significant drug resistance and leads to GEM treatment failure[16].

Herein, a visualisable photothermal controlled drug release nanosystem (VPNS) with a payload of phosphorylated GEM (pGEM) was developed to overcome the previously mentioned paradox (Scheme 1). To overcome GEM resistance in pancreatic cancer, pGEM, the active drug form, was directly used to circumvent insufficient activation of GEM in cancer cell metabolism. The photothermal effect generated from octabutoxyphthalocyanine palladium (II) (PdPc) in VPNS can release pGEM molecules captured by amphiphilic ligands, polyethylene glycol-poly(*Z*-lysine)-oleic acid (PEG-pLys(*Z*)-OA). Upon irradiation at 730 nm to induce the photothermal effect, pGEM can be released locally at the tumour site and simultaneous photothermal treatment in cancer cells can enhance the chemotherapeutic effect of pGEM.

[a] *Department of Interventional Radiology, Ruijin Hospital, Shanghai Jiao Tong University School of Medicine, 197, Rui Jin Er Road, Shanghai 200025, China.*
[b] *Institute of Biomedical Sciences, Department of Chemistry, Fudan University. 220 Handan Road, Shanghai 200433, China..*
[c] *Key Laboratory of Smart Drug Delivery, Ministry of Education, State Key Laboratory of Medical Neurobiology and MOE Frontiers Center for Brain Science, Department of Pharmaceutics, School of Pharmacy, Research Center on Aging and Medicine, Fudan University, 826 Zhangheng Road, Shanghai 201203, China.*
** Prof. Fuyou Li Email: fyli@fudan.edu.cn; Prof. Chen Jiang Email: jiangchen@shmu.edu.cn*
† Electronic Supplementary Information (ESI) available: See DOI: 10.1039/x0xx00000x

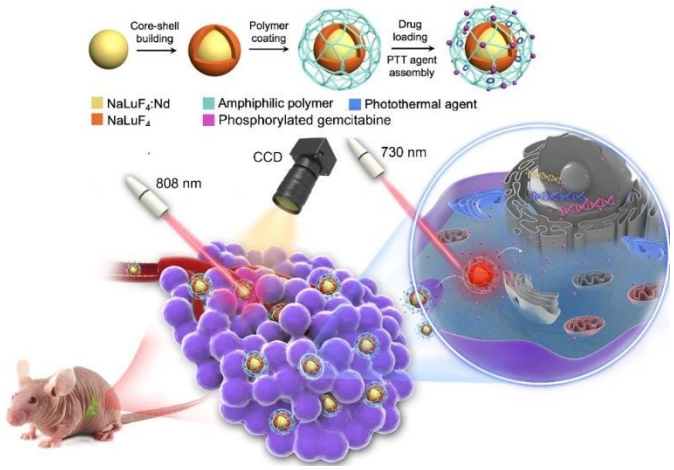

Scheme 1. To prepare the nanocarrier, a lanthanide-based nanoparticle was coated with amphiphilic ligands, PEG-pLys(Z)-OA. PdPc was loaded in the hydrophobic block (oleic acid) of PEG-pLys(*Z*)-OA and pGEM was loaded in the positively charged poly(*Z*-lysine) block of PEG-pLys(*Z*)-OA via electrostatic action. After intravenous injection of VPNS, an 808 nm laser was used to excite at ~1060 nm near-infrared luminescence to trace the drug distribution in the body. When the drug reaches the target tissue, 730 nm excitation realized the photothermal effect and promoted the release of the loaded drug in the target tissue, triggering local photothermal therapy.

2. Materials and Methods

2.1 Synthesis of pGEM and amphiphilic ligands

First, 1,2',2'-difluorodeoxycytidine (dFdC) was phosphorylated to 5'-monophosphate gemcitabine (pGEM) intracellularly, and an amphiphilic ligand was prepared in a stepwise manner, as shown in Scheme 1. A detailed synthesis strategy for these compounds is provided in the Supplementary Materials.

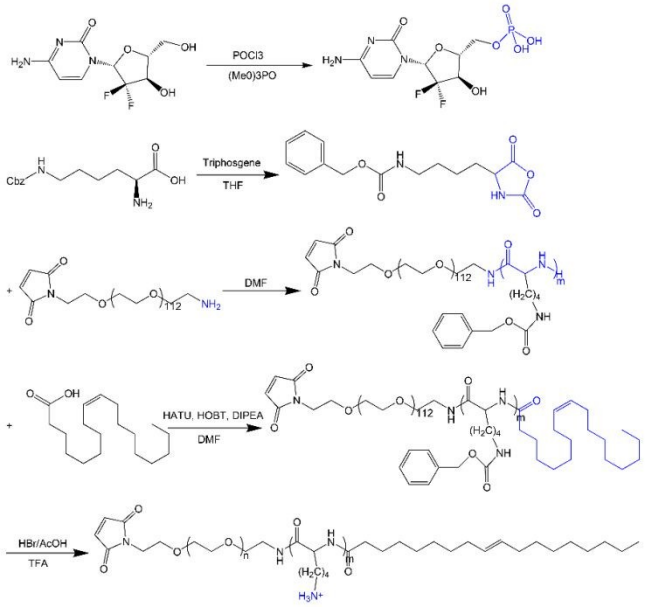

Scheme 2. Synthesis of pGEM and the amphiphilic ligand, polyethylene glycol-poly(Z-lysine)-oleic acid (PEG-pLys(Z)-OA).

2.2 Synthesis of the near infrared emissive lanthanide nanoparticles

For *in vivo* drug delivery and imaging, $NaLuF_4$:Nd@$NaLuF_4$ nanoparticles were synthesized as Nd^{3+} doped cores, exhibiting near infrared emission under the excitation of an 800 nm laser. Detailed synthetic methods of these nanoparticles are described in the Supplementary Materials.

2.3 Synthesis of octabutoxyphthalocyanine palladium (II) (PdPc)

To synthesize octabutoxyphthalocyanine palladium (II) (PdPc), 0.1 mmol of 1,4,8,11,15,18,22,25-octabutoxy-29H,31H-phthalocyanine and 0.3 mmol of $PdCl_2$ were added to 5 mL anhydrous dimethylformamide. The mixture was heated to 130 °C under N_2 protection for 24 h. When the mixture was cooled to 20 °C, 5 mL of methanol was added to precipitate PdPc. The product was washed using 10 mL of methanol to remove excess $PdCl_2$ and subsequently dried for further use.

2.4 Ligand coating and PdPc loading

$NaLuF_4$:Nd@$NaLuF_4$ or $NaLuF_4$:Yb,Er@$NaLuF_4$ nanoparticles coated with oleic acid (5 mg), PEG-pLys(*Z*)-OA (10 mg), and PdPc (4 mg) were co-dissolved in $CHCl_3$ (10 mL) and stirred at room temperature for 10 min. The solvent was removed by a rotary evaporator, to which flask deionized water (1.5 mL) was added to yield a dispersed suspension. The suspension was centrifuged (15000 rpm) for 10 min and the supernatant was subsequently removed. The solid was collected and re-suspended in deionized water (1.5 mL) to afford the nanoparticles modified with amphiphilic ligands.

2.5 Photothermal conversion efficiency

The photothermal conversion efficiency of the prepared nanocarrier was calculated under excitation with a 730 nm laser, according to a previously described method[17]. The detailed methods are provided in the Supplementary Materials.

2.6 Drug formulation and release

An aqueous solution (1.5 mL) containing the above drug loaded nanoparticles and pGEM (10^{-4} mol/L) was adjusted to pH 7.0 with NaOH (1 M) under stirring. The suspension was centrifuged (15,000 rpm) for 10 min and the supernatant was then removed. The solid was collected and re-suspended in deionized water (1.5 mL) to yield the drug-loaded nanoparticles. A UV-vis spectrometer was used to measure the pGEM remaining in the supernatant to calculate the drug loading rate. Drug-release kinetics were investigated under two parallel conditions: external temperature-controlled and photothermal-controlled drug release. A cuvette containing an aqueous solution of the drug-loading nanoparticles (0.5 mg/mL, 2 mL) was placed in an external temperature-controlled device, where the temperature was raised from 25 to 45 °C. At 5 °C intervals, 200 μL of the sample was extracted for centrifugation (15, 000 r/s, 10 min), where the upper supernatant was analysed by the UV-vis spectrometer for drug determination. For the photothermal-controlled drug release group, the NIR light power was set to 50 mW/cm^2, with a temperature increase from 25 to 45 °C. Each experiment was repeated three times to calculate the average and SD value.

2.7 Characterization of the drug-loading nanoparticles

Transmission electron microscopy (TEM) was used to observe the micromorphology and dispersity of the prepared

View Article Online
DOI: 10.1039/D0TB00017E

nanoparticles coated with oleic acid/ligand and drug-loading nanoparticles. Dynamic light scattering (DLS) was used to measure the size distribution and Zeta-potential of the empty and drug-loading nanoparticles. A UV-vis spectrometer was employed to determine the drug loading rate.

2.8 Antitumor efficacy *in vitro*

Mia Paca-2 cells were seeded in a 24-well plate with a 5×10^4 cells/well density and cultured overnight in an adherent state. GEM or pGEM (500 μL, 40 μg/mL) was added to the wells and cultured for 4 h. PBS was used to rinse the cells three times and DMEM (500 μL, containing 10% FBS) was added to each well. For the irradiated group, a 730-nm laser (180 mW/cm^2) was used to treat the cells for 10 min. All groups were cultured at 37 °C for 24 h and rinsed three times with PBS. Following the steps specified by the Annexin V-FITC kit, binding buffer (250 μL), Annexin V-FITC (2.5 μL), and propidium iodide (2.5 μL) was added subsequently. After 15 min, the medium was rinsed and the cells were observed via confocal microscopy, where the λex/em wavelengths for Annexin V-FITC and propidium iodide are 488/500–550 and 543/600–680 nm, respectively.

2.9 Animal preparation

The protocol used to establish an orthotopic nude mouse model of pancreatic cancer was reported previously[18]. All animals received human care in accordance with the National Institute of Health (NIH) Policy on the Care and Use of Laboratory Animals and the protocol was approved by the Animal Use and Care Committee of Ruijin Hospital, School of Medicine, Shanghai Jiaotong University.

2.10 *In vivo* distribution by IVIS

The *in vivo* distribution experiments were performed using mice with *in situ* pancreatic cancer 14 days post implantation. NGP (200 μL NGP, 5.0 mg/mL) was administrated via intravenous injection. After 6, 24, and 48 h, the IVIS system for small animals was applied to track the *in vivo* signal from $NaLuF_4$:Nd@$NaLuF_4$ nanoparticles, with an excitation wavelength of 808 nm and power of 200 mW/cm^2 with a 920 nm filer lens. D-luciferin in PBS (200 μL, 15 mg/mL) was injected into the mice to measure the in situ tumour volume and location in full-band acquisition mode after 10–15 min.

2.11 Anti-tumour efficacy *in vivo*

Tumour-bearing mice (24×) were divided into 6 groups: NGP+PTT (drug-delivery chemotherapy combined with photothermal therapy); NGP (drug-delivery chemotherapy); NP+PTT (photothermal therapy); NP (empty nanocarriers); GEM (commercial GEM); and NS (saline as a negative group).

Tumour-bearing mice were treated with GEM (20 mg/kg) or pGEM (26 mg/kg) via intravenous injection 10/14/18/22 days post tumour implantation, and the NGP+PTT/NP+PTT groups received photothermal treatment (λex=730 nm, 10 min, 200 mW/cm^2) 24 h after injection. All mice were observed under the IVIS Spectrum 10/17/24 days post implantation and the tumour signal was quantified using Living Image software 4.2. During the photothermal treatment and IVIS observation period, the mice were anaesthetized with isoflurane and monitored using a respiratory detector to avoid unexpected death. The detailed therapeutic strategy is illustrated in Scheme 3.

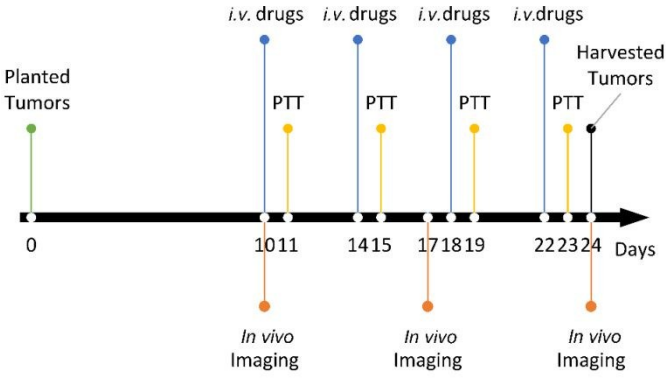

Scheme 3. The treatment was performed 10 days after tumour implantation, with a PTT 24 h after the drug-managed intravenous injection. If necessary, these treatments were repeated every 4 days. Luciferin bioluminescence imaging was performed every week to monitor tumour development.

Herein, the survival duration was not monitored because the PADC tumours of saline group grew so rapidly that after 3 weeks post implantation, they reached diameters of >2 cm. Considering the guideline request of Affidavit Animal Ethical Welfare, all mice were executed after 2 weeks and the anti-tumour effect was evaluated by comparing the excised tumour tissues. The tumour volume was calculated using the formula of long diameter multiplied by the square of the short diameter divided by 2.

2.12 Apoptosis tumour detection

Fluorescein labelled dUTP can link to the 3'-OH moiety of cleaved DNA in apoptosis tumour tissue under the action of the TdT enzyme and can be observed using fluorescence microscopy. Almost no 3'-OH DNA is observed in normal DNA and no fluorescein labelled dUTP can be formed. This strategy can be applied for detecting apoptosis in tumour cells.

The sliced samples were carefully marked prior to evaluation. PBS 7.4 (containing 4% paraformaldehyde) was used as a tissue fixation solution, PBS 7.4 (containing 1% Triton X-100) was used as a cellular membrane permeation fluid, and 3% H_2O_2 in PBS was used as a sealing fluid. The TdT enzyme solution was freshly prepared by adding FITC-12-dUTP (1.0 μL) and TdT enzyme (4.0 μL) into an equilibration buffer (45 μL) in the dark.

The TUNEL kit protocol was followed. Briefly, the air-dried sliced samples were immersed in tissue fixation solution and matured for 25 min at 25 °C, rinsed with PBS three times (5 min each). The samples were then immersed in the cellular membrane permeation fluid for 5 min and rinsed with PBS three times (5 min each). The samples were subsequently immersed in the sealing fluid for 10 min at 25 °C and rinsed with PBS three times (5 min each). The liquids of the samples were removed by bibulous paper. Each sample was mixed with TdT enzyme solution (50 μL) and covered with glass for 60 min at 37 °C. The samples were subsequently rinsed with PBS three times (5 min each). The samples were then stained with DAPI following a similar procedure.

2.13 Statistical analysis

STATA 14.0 software was used to analyse and present the data as means ± standard error (SD). Statistical comparisons were assessed by group *t*-tests and the accepted level of significance was $P < 0.05$.

3. Results

3.1 Synthesis and preparation of the nanoparticles

As shown in the TEM images, the as-synthesized $NaLuF_4$:Nd@$NaLuF_4$ core shell nanoparticles exhibited uniform and spherical morphologies with an average diameter of 28 nm (Fig. 1a). Upon coating of the $NaLuF_4$ shell layer on the $NaLuF_4$:Nd core, the emission at ~1060 nm showed a 4.3-fold enhancement (Fig. 1b). After coating of the PEG-pLys(*Z*)-OA and loading with PdPc, the DLS results showed a hydrated diameter of 50.8 nm (Fig. 1c) and Zeta-potential of +29 mV (Fig. 1d). Upon loading of pGEM, the Zeta-potential was changed to -20 mV (Fig. 1e), suggesting the successful absorption of pGEM. UV-vis spectroscopy was used to measure the residual pGEM at 268 nm in the solution after drug-loading, with an observed drug-loading rate of 55.6% (Fig. 1f).

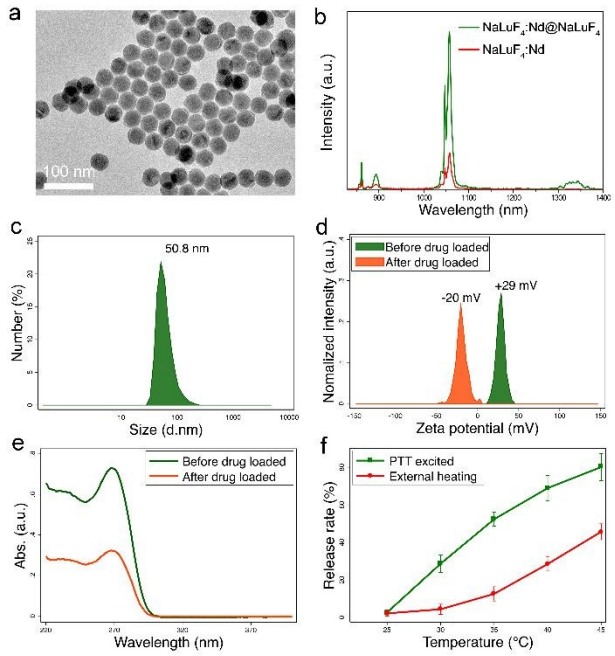

Figure 1. (a) TEM image of the $NaLuF_4$:Nd@$NaLuF_4$ core-shell nanoparticles. (b) Emission spectra of the $NaLuF_4$:Nd core and $NaLuF_4$:Nd@$NaLuF_4$ core-shell nanoparticles at 808 nm laser irradiation. (c) DLS measurement of $NaLuF_4$:Nd@$NaLuF_4$@PEG-pLys(Z)-OA loaded with PdPc and pGEM. The nanoparticles had a size distribution centred at approximately 50.8 nm. (d) Zeta-potentials of nanoparticles before (+29 mV) and after (-20 mV) pGEM loading. (e) UV absorption spectra of the pGEM supernatant before and after loading. The encapsulation efficiency of pGEM in VPNS was 55.6%. (f) pGEM release behaviour in VPNS upon 730 nm laser irradiation. The 730 nm laser can effectively trigger the release of pGEM at a relatively low external temperature compared to external heating.

Controlled drug release from the nanoparticles was also evaluated. The UV absorbance spectrum of the nanoparticles loaded with PdPc was first measured, showing a strong absorption at 730 nm (Supplementary Fig. 8). When the nanoparticles were heated to 35 °C with a heating shaker, the drug-release was 12.5% (Fig. 1e), suggesting relatively favourable stability in circulation. In contrast, when the system was heated to 45 °C with a 730 nm laser, the drug-release was as high as 80% due to the photothermal effect (Fig. 1e). The combined results indicated that the system achieved a controlled drug release upon non-invasive optical stimulation.

3.2 Antitumor efficacy *in vitro*

Cellular apoptosis of the MIA PaCa-2 pancreatic cancer cells induced by VPNS loaded with pGEM and photothermal treatment (NPG+PTT), VPNS loaded with pGEM alone (NPG), VPNS without pGEM and photothermal treatment (NP+PTT), VPNS without pGEM (NP), GEM, and NS was examined by fluorescence microscopy after 4 h of treatment and a further 24 h of incubation. As shown in Fig. 2, the NPG+PTT group exhibited an earlier apoptosis (stained with ANNEXIN V) as well as late apoptosis (stained with PI) compared to the other groups, indicating the most obvious antitumor efficacy. In contrast, the NPG and NP+PTT groups showed less antitumor efficacy. The NP, GEM, and saline groups caused nearly no cell apoptosis in the period tested.

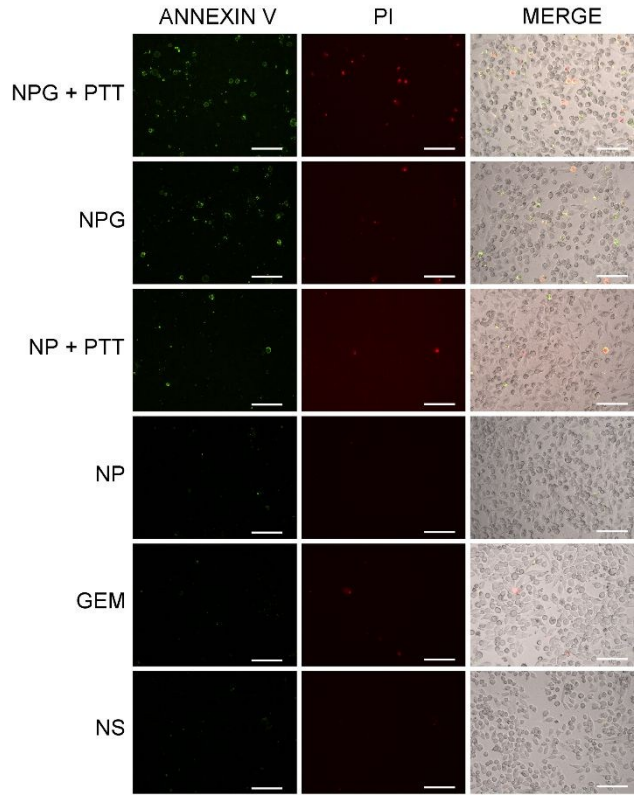

Figure 2. Anti-tumour efficacy of the nanocarrier *in vitro*. Apoptotic cells were labelled with the Annexin V-FITC Apoptosis Detection Kit. Green: FITC labelled phosphatidylserine. Red: PI labelled nucleus. Scale bar = 50 μm. Original magnification: ×100.

3.3 Biodistribution *in vivo*

In this strategy, Nd in $NaLuF_4$:Nd@$NaLuF_4$ nanoparticles absorb at 808 nm and emit at ~1060 nm to realize an *in vivo* bioimaging. As shown in Fig. 3, luciferase labelled by fluorescein (green) can

be used to determine the location and size of the tumour, while the red signal yields the biodistribution information of the nanoparticles. After 6 h post intravenous injection, the nanoparticles mainly accumulated in the liver and spleen, whereas 24 h post injection, the nanoparticles further accumulated in the tumour. After 48 h post the injection, the nanoparticles were mainly located in liver, spleen, and intestinal tract (possibly due to enterohepatic circulation). Based on these findings, the peak concentration of the nanoparticles in the tumour was observed around 24 h, which was selected for further photothermal effect and photothermal-initiated drug release testing (Scheme 3).

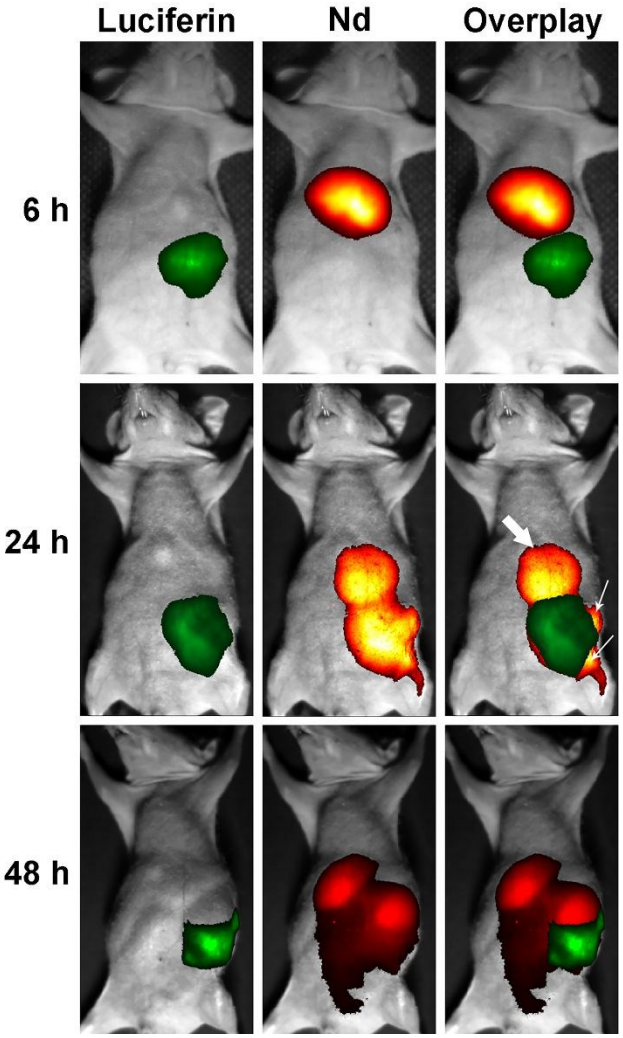

Figure 3. *In vivo* imaging of model mice with orthotopic xenograft tumours of pancreatic cancer administrated with nanoparticles. Green: luciferase; Fire red: NaLuF4:Nd@NaLuF4; Thick arrow: liver; Thin arrow: spleen.

Increased drug concentration in the tumour tissue is a key factor that affects antitumor efficacy, especially for pancreatic cancer, where the penetration of chemodrugs have been greatly limited by the extensive tumour stroma[19, 20]. Several strategies have been developed to increase the drug distribution in other tumours, such as active targeting[21-23]. However, pancreatic cancer cells lack available targeting receptors for active targeting ligands due to their high heterogeneity[16, 24]. Compared to the active targeting strategy, physically enhanced penetration should be more reliable. The passive targeting strategy used herein can prolong the circulation of the nanomedicine and achieve a higher accumulation in tumours *via* the EPR effect. The distribution of the nanoparticles in liver and spleen should not be neglected, but the strategy of photothermal-initiated local drug release could elevate the distribution of loaded agents in the tumour and while reducing the active content in normal tissue.

3.4 Antitumor efficacy *in vivo*

The therapy used herein was started 10 days post tumour implantation, and at the 17th and 24th day, luciferase bioluminescence was used to measure tumour size variation, which was semi-quantified and shown in Fig. 4. Among all the treatment groups, the tumour inhibition during the early stages of the combined nanoparticles and PTT group was the most significant. It should be noted that as the treatment proceeded, tumour recurrence occurred in the later stages, but this was much milder than in the control groups. This was ascribed to the residual tumour cells in deeper tissues that were difficult to completely eliminate using the 730 nm laser. The signal quantification from the entire abdominal region of each mouse demonstrated the above tendency, as shown in Supplementary Fig. S10.

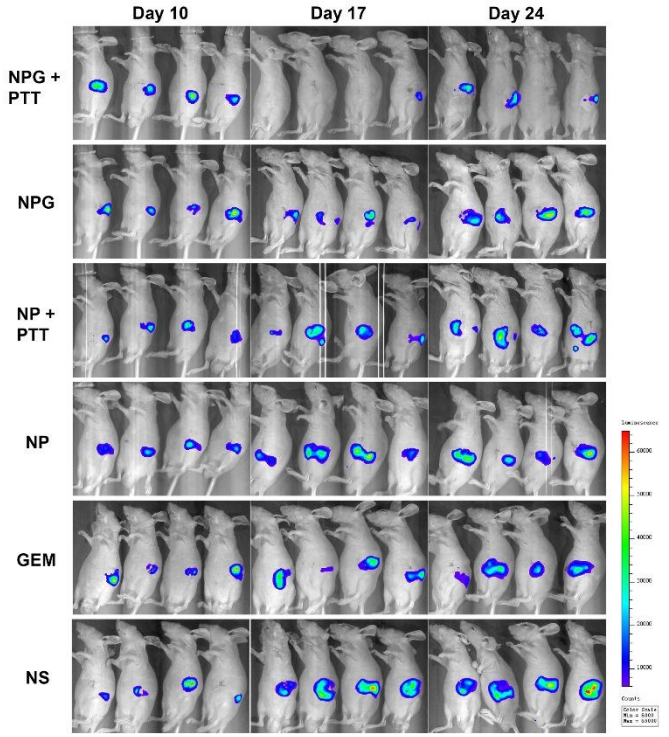

Figure 4. Non-invasive bioluminescence imaging of tumour bearing mice. Mice with orthotopic xenograft tumours of pancreatic cancer received a dose of 20 mg/kg-equiv. GEM injection on 10/14/18/22 days after tumour implantation, where the NGP+PTT/NP+PTT groups received photothermal treatment. The bioluminescence imaging was performed three times on days 10/17/24.

The animal model of pancreatic cancer used herein was an orthotopic pancreatic tumour and the tumour size was difficult

View Article Online
DOI: 10.1039/D0TB00017E

to accurately measured *in vivo*. The mice were sacrificed and the isolated tumours are shown in Fig. 5a. The tumour volume (mm^3) of the NPG combined with photothermal treatment group was statistically different from those of the other groups (Fig. 5b). Apoptosis of the tumour cells was stained by terminal deoxynucleotidyl transferase dUTP nick end labelling (TUNEL). As shown in Fig. 5c, many apoptotic cells (green) were detected in the NPG+PTT, NPG, and NP+PTT groups. Moreover, the signal intensity in the NPG+PTT group was much higher, whereas almost no apoptosis signal was observed in the other groups.

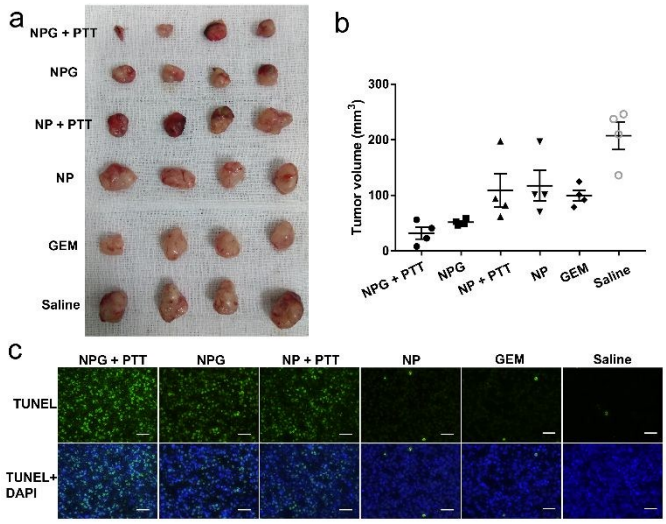

Figure 5. Anti-tumour efficiency *in vivo*. (a) Tumours harvested from the mice treated with NPG + PTT, NPG, NP + PTT, NP, GEM, and NS. (b) The distribution of tumour volumes for mice. (c) TUNEL staining was used to detect cell apoptosis in the tumours, wherein green is FITC labelled dUTP indicating apoptotic cells and blue is the nucleus stained by DAPI. Scale bar = 50 μm. Original magnification: ×100.

4. Discussion

Herein, pGEM was synthesized to overcome the drug resistance of pancreatic cancer cells. A visualizable nanosystem was designed to escort the pGEM for pancreatic cancer therapy in real-time monitoring mode. The nanosystem achieved a photothermal effect with an NIR laser to trigger local drug release to enhance the therapeutic effect. The drug activity was demonstrated *in vitro* and *in vivo*. The synergy of the two different therapeutic modalities (chemotherapy and photothermal therapy) is a promising approach to overcome the limitation of single treatment modalities to achieve enhanced therapeutic outcomes.

Because few clinical signs or symptoms are evident during the early stages of pancreatic cancer and disease-specific biomarkers remain unknown, early detection is extremely difficult. Only 30% pancreatic cancer patients have a chance of exairesis, and for most patients in advanced stage, cytotoxic drugs remain the gold standard in therapy[6, 25]. In 1996, GEM was approved for clinical PDAC therapy and only the FOLFIRINOX strategy showed advantageous effects, but suffers from serious side-effects since FOLFIRINOX combines four drugs[26]. In 2013, Vof et al.[11] developed a protocol using GEM plus ABRAXANE (albumin bound paclitaxel), showing a significantly increased median survival time of 8.5 months, which has become the first-line treatment for PDAC[27, 28].

Therefore, GEM plays a key role in PDAC treatment, but it must be phosphorylated into the therapeutic species (pGEM). In tumour cells, the crucial transformation catalysis via deoxycytidylate kinase is often deactivated, limiting the formation of pGEM[29]. Once pGEM enters the tumour cell, it is reversibly transformed into di- or tri-phosphorylated GEM, which exerts an anti-tumour effect [30]. In contrast, the rich matrix in PDAC and the corresponding high pressure greatly reduces blood perfusion, resulting in a low GEM concentration[31]. In addition, the acquired heterogeneity during the PDAC evolution and progress increases resistance to GEM therapy, which is also an important factor leading to treatment failure[16]. Overcoming the above limitations will greatly advance the quality of PDAC clinical treatment.

Based on the analysis of the structure-property relationships, pGEM contains many negative charges, which could be used as an interaction mechanism for pGEM loaded nanomedicine. Thus, an amphiphilic ligand was designed to modify the nanoparticles to reduce RES (reticuloendothelial system) ingestion and prolong circulation time. The ligand with a positively charged moiety from lysine residues can absorb and escort pGEM to the tumour *via* the EPR effect. PADC tumours lack available receptors that can be used for active targeting with nanomedicines. Therefore, using the EPR effect is a useful accumulation tactic[32, 33]. At present, lots of researches about drug delivery of gemcitabine have been reported with the aims of smart or combined drug delivery[34], but relatively few studies focus on phosphorylated GEM[35, 36]. In this study, the activated gemcitabine was loaded with electrostatic adsorption and released with photothermal effect to overcome the resistance of pancreatic cancer due to GEM phosphorylation barrers intracellularly. However, from the experimental results, unexpected accumulation in the liver and spleen should be considered prior to clinical translation.

The NIR II nanoparticles are useful for tracking the drug distribution to guide drug release via the photothermal effect upon NIR laser irradiation. Though several studies using NIR I (< 800 nm) emitting nanomaterials have demonstrated imaging guided drug release in subcutaneous tumour models, it remains unclear if these results reflect clinical situations because *in situ* PDAC normally exists in deeper tissues than can be irradiated. In other words, previous studies using subcutaneous tumour models and shorter wavelength emission (<800 nm) cannot easily be translated into the clinic. Herein, a 1100 nm luminescence (NIR II window) and orthotopic tumour model were used to demonstrate imaging-guided cancer therapy with a high possibility of clinical translation. In subsequent studies, interventional therapy will be adopted by introducing an optical fibre into the orthotopic tumours to enhance the photothermal effect.

Nanoparticle-based photothermal therapy has received extensive attention for the treatment of cancer[37-39]. Herein, the combination of chemotherapy and photothermal therapy with VPNS produced favourable anti-tumour effects. Previous studies have demonstrated that the microscopic temperature

of the nanoparticle increases significantly during photothermal activation without inducing large changes in the ambient temperature[17], which is applicable to the nanosystem studied herein. The microscopic temperature of VPNS during the photothermal process can be used to induce drug release in real-time. Simultaneously, the photothermal effect enhances the selectivity of the cytotoxic drug, further improving the therapeutic effect, which can also be monitored by microscopic temperature measurement.

4. Conclusion

Herein, a lanthanide-based visualizable photothermal controlled drug release nanosystem was developed for pancreatic cancer treatment. An amphiphilic ligand was prepared to coat the nanoparticles to prolong circulation and load pGEM. The nanoparticles effectively accumulated in the tumour as monitored by *in vivo* bioimaging to measure real-time drug distribution. Upon NIR light irradiation, the nanosystem showed an obvious photothermal effect to initiate pGEM release. The anti-tumour effect of the prepared nanosystem was demonstrated both *in vitro* and *in vivo*. This study can provides a novel therapeutic strategy for PDAC that has a high probability of success in the clinic.

Abbreviations

dFdC: 1,2',2'-difluorodeoxycytidine; DLS: dynamic light scattering; GEM: gemcitabine; NIR: near infrared; NP: empty nanocarriers; NP+PTT: photothermal therapy; NPG: drug-delivery chemotherapy; NPG+PTT: drug-delivery chemotherapy combined with photothermal therapy; NS: saline; PDAC: pancreatic ductal adenocarcinoma cancer; PdPc: octabutoxyphthalocyanine palladium (II); PEG-pLys(Z)-OA: polyethylene glycol-poly(Z-lysine)-oleic acid; pGEM: phosphorylated GEM; SD: standard error; TEM: Transmission electron microscopy; VPNS: visualisable photothermal controlled drug release nanosystem;

Conflicts of interests:

The authors have declared that no competing interest exists.

Acknowledgements

This work supported by grants from the Shanghai Municipal Key Clinical Specialty (shslczdzk06002 and shslczdzk07002).

References

1. L. A. Torre, F. Bray, R. L. Siegel, J. Ferlay, J. Lortet-Tieulent and A. Jemal, *CA: a cancer journal for clinicians*, 2015, **65**, 87-108.

2. T. Kamisawa, L. D. Wood, T. Itoi and K. Takaori, *Lancet (London, England)*, 2016, **388**, 73-85.

3. L. D. Mellby, A. P. Nyberg, J. S. Johansen, C. Wingren, B. G. Nordestgaard, S. E. Bojesen, B. L. Mitchell, B. C. Sheppard, R. C. Sears and C. A. K. Borrebaeck, *International journal of cancer*, 2018, **36**, 2887-2894.

4. D. P. Ryan, T. S. Hong and N. Bardeesy, *The New England journal of medicine*, 2014, **371**, 2140-2141.

5. W. Hartwig, J. Werner, D. Jager, J. Debus and M. W. Buchler, *The Lancet. Oncology*, 2013, **14**, e476-e485.

6. O. Strobel and J. Neoptolemos, 2019, **16**, 11-26.

7. J. Bukki, *The New England journal of medicine*, 2014, **371**, 2139-2140.

8. A. Arshad, D. Al-Leswas, O. Al-Taan, J. Stephenson, M. Metcalfe, W. P. Steward and A. R. Dennison, *American journal of clinical oncology*, 2013, **36**, 411-414.

9. H. A. Burris, 3rd, M. J. Moore, J. Andersen, M. R. Green, M. L. Rothenberg, M. R. Modiano, M. C. Cripps, R. K. Portenoy, A. M. Storniolo, P. Tarassoff, R. Nelson, F. A. Dorr, C. D. Stephens and D. D. Von Hoff, *Journal of clinical oncology : official journal of the American Society of Clinical Oncology*, 1997, **15**, 2403-2413.

10. M. J. Moore, D. Goldstein, J. Hamm, A. Figer, J. R. Hecht, S. Gallinger, H. J. Au, P. Murawa, D. Walde, R. A. Wolff, D. Campos, R. Lim, K. Ding, G. Clark, T. Voskoglou-Nomikos, M. Ptasynski and W. Parulekar, *Journal of clinical oncology : official journal of the American Society of Clinical Oncology*, 2007, **25**, 1960-1966.

11. D. D. Von Hoff, T. Ervin, F. P. Arena, E. G. Chiorean, J. Infante, M. Moore, T. Seay, S. A. Tjulandin, W. W. Ma, M. N. Saleh, M. Harris, M. Reni, S. Dowden, D. Laheru, N. Bahary, R. K. Ramanathan, J. Tabernero, M. Hidalgo, D. Goldstein, E. Van Cutsem, X. Wei, J. Iglesias and M. F. Renschler, *The New England journal of medicine*, 2013, **369**, 1691-1703.

12. Z. Wang, Y. Li, A. Ahmad, S. Banerjee, A. S. Azmi, D. Kong and F. H. Sarkar, *Nature reviews. Gastroenterology & hepatology*, 2011, **8**, 27-33.

13. A. Rajabpour, F. Rajaei and L. Teimoori-Toolabi, *Pancreatology : official journal of the International Association of Pancreatology (IAP) ... [et al.]*, 2017, **17**, 310-320.

14. B. Uzunparmak and I. H. Sahin, *Clinical and translational medicine*, 2019, **8**, 2.

15. Z. Han and Z.-R. Lu, *J Mater Chem B*, 2017, **5**, 639-654.

16. J. Cros, J. Raffenne, A. Couvelard and N. Pote, *Pathobiology : journal of immunopathology, molecular and cellular biology*, 2018, **85**, 64-71.

17. X. Zhu, W. Feng, J. Chang, Y.-W. Tan, J. Li, M. Chen, Y. Sun and F. Li, *Nature Communications*, 2016, **7**, 10437.

18. Q. Wang, J. Li, S. An, Y. Chen, C. Jiang and X. Wang, *International journal of nanomedicine*, 2015, **10**, 4479-4490.

19. X. Chen, W. Zhou, C. Liang, S. Shi, X. Yu, Q. Chen, T. Sun, Y. Lu, Y. Zhang, Q. Guo, C. Li, Y. Zhang and C. Jiang, 2019, DOI: 10.1021/acs.nanolett.9b00374.

20. T. Murakami, Y. Hiroshima, R. Matsuyama, Y. Homma, R. M. Hoffman and I. Endo, 2019, **3**, 130-137.

21. Y. Pei, L. Chen, Y. Huang, J. Wang, J. Feng, M. Xu, Y. Chen, Q. Song, G. Jiang, X. Gu, Q. Zhang, X. Gao and J. Chen, *Small (Weinheim an der Bergstrasse, Germany)*, 2019, **15**, e1900631.

22. X. Chen, W. Zhou, C. Liang, S. Shi, X. Yu, Q. Chen, T. Sun, Y. Lu, Y. Zhang, Q. Guo, C. Li, Y. Zhang and C. Jiang, *Nano letters*, 2019, **19**, 3527-3534.

23. A. Banstola, T. T. Pham, J. H. Jeong and S. Yook, *Drug delivery*, 2019, **26**, 629-640.

24. B. El Hassouni, G. Li Petri, D. S. K. Liu, S. Cascioferro, B. Parrino, W. Hassan, P. Diana, A. Ali and A. E. Frampton, 2019, **15**, 437-447.

25. K. J. Labori, K. Lassen, D. Hoem, J. E. Gronbech, J. A. Soreide, K. Mortensen, R. Smaaland, H. Sorbye, C. Verbeke and S. Dueland, *BMC surgery*, 2017, **17**, 94.

26. T. Conroy, F. Desseigne, M. Ychou, O. Bouche, R. Guimbaud, Y. Becouarn, A. Adenis, J. L. Raoul, S. Gourgou-Bourgade, C. de la Fouchardiere, J. Bennouna, J. B. Bachet, F. Khemissa-Akouz, D. Pere-Verge, C. Delbaldo, E. Assenat, B. Chauffert, P. Michel, C. Montoto-Grillot and M. Ducreux, *The New England journal of medicine*, 2011, **364**, 1817-1825.

27. A. McBride, M. Bonafede, Q. Cai, N. Princic, O. Tran, C. Pelletier, M. Parisi and M. Patel, *Expert review of clinical pharmacology*, 2017, **10**, 1153-1160.

28. J. Kang, I. Hwang, C. Yoo, K. P. Kim, J. H. Jeong, H. M. Chang, S. S. Lee, D. H. Park, T. J. Song, D. W. Seo, S. K. Lee, M. H. Kim, S. M. Hong, S. H. Shin, D. W. Hwang, K. B. Song, J. H. Lee, S. C. Kim and B. Y. Ryoo, *Investigational new drugs*, 2018, **36**, 732-741.

29. M. Amrutkar and I. P. Gladhaug, 2017, **9**.

30. E. J. B. Derissen, A. D. R. Huitema, H. Rosing, J. H. M. Schellens and J. H. Beijnen, *British journal of clinical pharmacology*, 2018, **84**, 1279-1289.

31. P. Dauer, A. Nomura, A. Saluja and S. Banerjee, *Pancreatology : official journal of the International Association of Pancreatology (IAP) ... [et al.]*, 2017, **17**, 7-12.

32. D. N. Khalil and E. M. O'Reilly, *Clinical cancer research : an official journal of the American Association for Cancer Research*, 2018, **24**, 4355-4356.

33. A. D. Singhi, E. J. Koay, S. T. Chari and A. Maitra, *Gastroenterology*, 2019, **156**, 2024-2040.

34. H. Meng, M. Wang, H. Liu, X. Liu, A. Situ, B. Wu, Z. Ji, C. H. Chang and A. E. Nel, *ACS nano*, 2015, **9**, 3540-3557.

35. W. S. Loc, S. S. Linton, Z. R. Wilczynski, G. L. Matters, C. O. McGovern, T. Abraham, T. Fox, C. M. Gigliotti, X. Tang, A. Tabakovic, J. A. Martin, G. A. Clawson, J. P. Smith, P. J. Butler, M. Kester and J. H. Adair, *Nanomedicine : nanotechnology, biology, and medicine*, 2017, **13**, 2313-2324.

36. T. H. Senanayake, G. Warren, X. Wei and S. V. Vinogradov, *Journal of controlled release : official journal of the Controlled Release Society*, 2013, **167**, 200-209.

37. M. Farokhi, F. Mottaghitalab, M. R. Saeb and S. Thomas, *Journal of controlled release : official journal of the Controlled Release Society*, 2019, DOI: 10.1016/j.jconrel.2019.07.036.

38. D. de Melo-Diogo, R. Lima-Sousa, C. G. Alves and I. J. Correia, *Biomaterials science*, 2019, DOI: 10.1039/c9bm00577c.

39. Y. Zhang, N. Song, Y. Li, Z. Yang, L. Chen, T. Sun and Z. Xie, *J Mater Chem B*, 2019, **7**, 4717-4724.

View Article Online
DOI: 10.1039/D0TB00017E

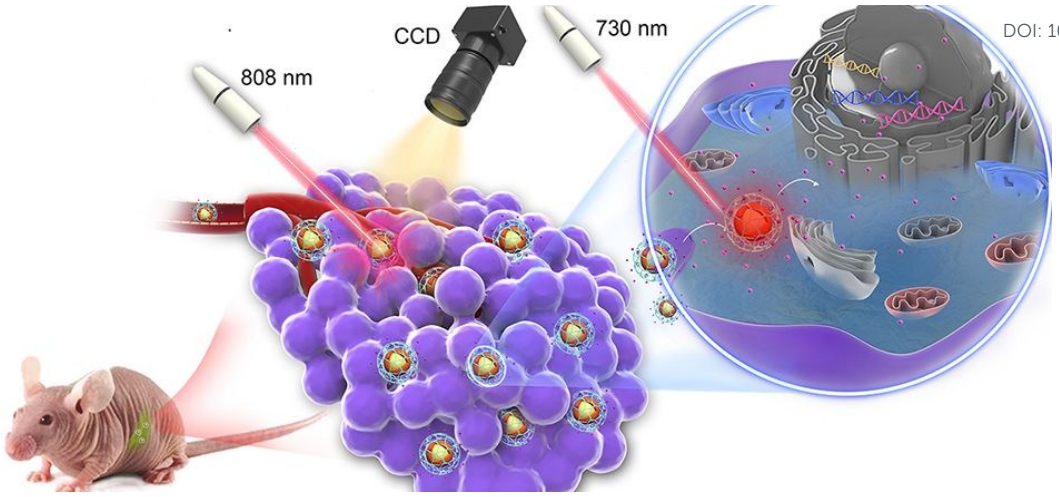

A lanthanide-based visualizable photothermal controlled drug release nanosystem was developed to overcome the drug resistance of gemcitabine for pancreatic cancer.